THE ASTROPHYSICAL JOURNAL SUPPLEMENT SERIES, 94:147–162, 1994 September

THE MOLECULAR EMISSION-LINE SPECTRUM OF IRC +10216 BETWEEN 330 AND 358 GHZ

T. D. GROESBECK AND T. G. PHILLIPS
Division of Physics, Mathematics and Astronomy, California Institute of Technology, 320-47, Pasadena, CA 91125
AND
GEOFFREY A. BLAKE
Division of Geological and Planetary Sciences, California Institute of Technology, 170-25, Pasadena, CA 91125
Received 1993 September 14; accepted 1994 February 7

ABSTRACT

We have conducted a spectral line survey of IRC +10216 using the Caltech Submillimeter Observatory to an average sensitivity of $\lesssim$95 mK. A deconvolution algorithm has been used to derive the continuous single-sideband spectrum from 330.2 to 358.1 GHz. A total of 56 spectral lines were detected of which 54 have been identified with 8 molecules and a total of 18 isotopomers. The observed lines are used to derive column densities and relative abundances for the detected species. Within this frequency range the spectral lines detected contribute the majority of the total flux emitted by IRC +10216. We use the derived column densities and excitation temperatures to simulate the molecular line emission (assuming LTE) at frequencies up to 1000 GHz. The observed and simulated flux from line emission is compared to broadband total flux measurements and to dust emission assuming a power-law variation of the dust emissivity. We conclude that significant corrections for the line flux must be made to broadband flux measurements of IRC +10216 at wavelengths longer than $\sim$750 μm.

Subject headings: circumstellar matter — line: identification — radio lines: ISM — stars: individual (IRC +10216)

1. INTRODUCTION

During the past several years, new high-sensitivity submillimeter telescopes and receivers have become operational, allowing astronomical observations to be carried out in previously inaccessible regions of the spectrum. This paper presents the continuation of a program of comprehensive molecular line surveys, initiated with the earlier studies of Orion-KL (Sutton et al. 1985; Blake et al. 1986). We have continued these studies at higher frequencies and have extended the observations to include a more diverse set of objects. In this paper we display the 1 mm spectrum of IRC +10216 and discuss the effects of line emission on broadband flux measurements.

The carbon star IRC +10216 has been extensively studied at infrared and millimeter wavelengths. First noted as one of the brightest objects in the sky at 5 μm (Becklin et al. 1969), it is an evolved star with an extended circumstellar envelope of gas and dust (the CO J = 1–0 and 2–1 lines are detected out to a radius of $\gtrsim$200″; Huggins, Olofsson, & Johansson 1988) expanding at a roughly constant velocity of 14.5 km s^{-1}. The molecular line emission from the circumstellar envelope reveals a carbon-rich chemistry that is generally understood in terms of a model where near equilibrium abundances in the warm inner regions "freeze out" (McCabe, Smith, & Clegg 1979) as the temperature cools with increasing distance from the star, and are then modified by photochemistry in the outer regions of the envelope (e.g., Glassgold et al. 1987).

A rich spectrum of molecular lines has been observed from IRC +10216 at millimeter and submillimeter wavelengths. Many species have been seen first or in some cases only in IRC +10216 (e.g., SiCC, Thaddeus, Cummins, & Linke 1984; NaCl, AlCl, KCl, AlF, Cernicharo & Guélin 1987). Johansson et al. (1984) performed a spectral survey of IRC +10216 from 72 to 93 GHz detecting 12 species as well as many of the corresponding isotopic variants. An unpublished survey using the IRAM 30 m telescope has been collected including large portions of the spectrum between 3 and 1.3 mm, from which several detections of new and unusual molecules have been published (cf. Cernicharo et al. 1991). Avery et al. (1992) have recently published a survey from the 15 m JCMT covering the interval from 339.6 to 364.6 GHz as well as a range of 14.2 GHz distributed between 222.4 and 267.9 GHz with the spectra presented in double sideband (DSB) form. We present here a spectral line survey of IRC +10216, performed with the 10.4 m telescope of the Caltech Submillimeter Observatory[1] (CSO), covering the range from 330.2 to 358.0 GHz with significantly greater sensitivity than that of the survey by Avery et al. and which has been reduced to give the spectrum in a single sideband (SSB) format. A total of 56 emission lines are seen in our data; with the exception of two features, all are identified with molecules which have previously been observed in IRC +10216.

There are several predictable differences between this survey and work at lower frequencies (cf. Jewell et al. 1989; Sutton et al. 1991; Avery et al. 1992). The heavier rotors (e.g., HC_3N, HC_5N) which displayed strong emission near 3 mm are no longer seen at 0.87 mm, while the emission from lighter molecules, particularly diatomics, is significantly increased as is expected from consideration of the rotational partition functions and level populations. Several molecules also exhibit emission in vibrationally excited states, a result of the increased optical depths at submillimeter frequencies under IR pumping. Finally, the emission lines near 345 GHz contribute an increased

[1] The Caltech Submillimeter Observatory is funded by the National Science Foundation under contract AST-9015755.

and substantial fraction of the broadband flux detected from IRC +10216.

2. OBSERVATIONS AND DATA REDUCTION

2.1. *Observations*

The observations for the survey were obtained during several periods between 1989 January and 1992 January using the 10.4 m CSO telescope located on Mauna Kea, Hawaii. Table 1 lists the observing dates together with the approximate frequency ranges covered for each observing session. The data were taken in an overlapping fashion with many frequencies observed at more than one epoch. The variations in the observed line intensities between different sessions were comparable to the variations seen during a single session; in the deconvolution method used to derive the final spectrum it was assumed that the actual intensities were constant for all of the observations. The CSO telescope had a FWHM beamwidth of 20″ averaged over the range of frequencies observed. Pointing was checked frequently, using observations of planets as well as observations of strong lines of species with compact emission from IRC +10216 itself, and was found to be accurate to $\lesssim 5''$.

An SIS receiver (Ellison et al. 1989) was used in DSB mode, and the SSB spectrum was reconstructed using an algorithm described below. Receiver temperatures were typically 200–250 K (SSB), and total system temperatures ranged from 700 to 2000 K (SSB). The atmospheric opacity was generally less than 0.25, but reached 0.6 on a few occasions. An acousto-optic spectrometer with a bandwidth of 500 MHz and a nominal channel width of 0.49 MHz served as the backend. The SSB spectrum is reconstructed with 1 MHz channels, giving a velocity resolution which varies from 0.91 to 0.84 km s^{-1} over the frequencies observed. For the bulk of the survey, the observations yielded an rms noise level of 65 mK (main beam temperature units) per channel. Because of time constraints, we were unable to achieve a uniform sensitivity over the entire frequency range. In particular, the frequency regions 332.7–333.0 GHz, 337.0–338.0 GHz, and 338.5–339.2 GHz exhibit significantly higher noise levels than the rest of the frequency range observed. We have therefore smoothed the data in those regions to a resolution of 4 MHz per channel, giving an rms noise level of 95 mK for these channels. Since nearly all lines from this source are observed to have widths of $\sim$30 km s^{-1} (34 MHz at 340 GHz), the smoothing should not significantly affect the detection of any lines in these regions, although the line profiles will be less well determined.

TABLE 1

OBSERVING DATES AND FREQUENCIES

Dates	Frequencies [a] (GHz)
1989 January 18–21	341–346
1989 April 25–May 3	340–341,343-349
1990 January 14–17	345–350
1990 March 13–19	330–331,333–336,337–340,351–358
1991 January 7–13	331–340,342–343,346–351
1992 January 11	352–358 [b]

[a] Approximate frequency ranges covered during each observing session.

[b] Several small regions within this range were observed to complete the continuous spectrum.

The chopper wheel method was used to calibrate the data at the time of the observations (Penzias & Burrus 1973). Low-order polynomial baselines were then removed from the observed DSB spectra. For frequencies near the ends of the survey where the atmospheric transmission varies rapidly with frequency, the different atmospheric opacities in the two sidebands were modeled (Grossman 1989) to allow corrections to be made to the observed antenna temperatures. The data presented here have been corrected by the main beam efficiency of $\eta_{MB} = 0.6$ as determined from planetary measurements. Because the line emission arises from regions of different angular extent for different molecules, the use of a single efficiency correction will result in some errors in the resulting brightness temperatures, particularly for very extended or very compact emission. For comparison, the extended efficiency was found to be $\eta_{ext} = 0.76$ from observations of the Moon. We estimate the uncertainties in the absolute calibration to be 20% because of potential errors in the chopper wheel calibration, in the efficiency measurements, and in the sideband gain determinations.

2.2. *Deconvolution Method*

Previous authors have taken various approaches to the problem of presenting spectral survey data when the observations were made using DSB receivers. Turner (1989) simply added together the DSB spectra which covered each frequency, not including those that contained emission attributed to the other sideband, and presented the SSB spectrum obtained in this manner. The method presented by Greaves & White (1991) is essentially an extension of this approach. The final spectrum is determined first for regions that are free of line emission in individual scans. These values are then used to determine the spectrum at corresponding frequencies in the opposite sideband in other scans. Jewell et al. (1989) and Avery et al. (1992) present DSB spectra covering the range of their survey, with Jewell et al. including observations at slightly shifted frequencies in order to resolve sideband ambiguities.

Sutton et al. (1985), and later Blake et al. (1986), used a modification of the CLEAN algorithm for deconvolving aperture synthesis maps to combine their DSB observations into a SSB spectrum for the range of frequencies covered. The current data set has been reduced using a similar implementation of the CLEAN algorithm. First, a "dirty" spectrum was generated by combining the DSB observations and including contributions from both sidebands at each frequency. After the strongest line in the dirty spectrum was found, a small fraction ($\sim$0.2) of its strength was subtracted from the dirty spectrum, and that amount was added to the "clean" spectrum. Properly scaled amounts were also subtracted at all of the image frequencies in the dirty spectrum (corresponding to the image sideband of each DSB spectrum containing the line frequency in the signal sideband). This process was then repeated until the noise level in the data was reached. By contrast, the earlier implementation of Sutton et al. and Blake et al. performed the iterative subtractions on the individual DSB spectra rather than on the dirty spectrum, and required a new dirty spectrum

to be generated at regular intervals as the DSB spectra changed. A greater than tenfold increase in processing speed resulted from our modifications.

Blake et al. (1986) found that increasing the overlap between DSB observations to increase the number of times each frequency was observed improved the performance of the CLEAN algorithm. Following their approach, we generally took spectra centered at intervals of 250 MHz or half the backend width, so that each frequency would be observed twice in the lower sideband and twice in the upper sideband in the interior regions of the survey. This redundancy was important in reducing the ambiguities caused by overlapping lines in individual spectra. In some cases additional scans were acquired with the local oscillator shifted by 10 or 20 MHz to aid in the assignment of spectral features to a particular sideband while the observations were being made. These small shifts in frequency also provided important additional redundancy near the edges of the survey where lines were not observed in both sidebands.

We have performed numerical tests using simulated data to investigate the ability of the modified CLEAN algorithm to accurately reconstruct a SSB spectrum from DSB observations. These simulations and our experience with the present data set (as well as data sets from other surveys) indicate that the accuracy of the SSB spectrum is limited by the noise in the original data and that the processing does not introduce additional errors. While a unique SSB spectrum cannot be determined from a set of DSB observations, the simplicity of the spectrum for the current data set makes it likely that the presented spectrum is correct. The generally uncrowded spectrum combined with the easily recognizable line shapes make it easy to verify the presence of lines in the original DSB observations. All of the spectral features labeled in the present data were visible in the DSB scans, although they were sometimes blended.

The CLEAN algorithm assumes that each observation of a line results in identical measurements and subtracts scaled versions of the real line from its images. Any variation in the line profile or intensity in different observations will result in incomplete subtraction of the images, leaving "ghosts" at the image frequencies. Possible sources of variations in an observed line include uncertainties in the sideband gain ratios, pointing errors, calibration errors and noise, as well as actual variations in the line intensity between different epochs. Errors that produce a simple scaling of the line, such as sideband gain ratios different from unity, can be corrected by scaling the amounts subtracted. Errors such as pointing errors which produce a different line shape cannot be completely corrected and result in ghosts. For the present data, the sideband ratios have been found to vary typically by less than 15%. The multiple observations of the lines allow the sideband gains to be estimated sufficiently accurately to eliminate gain variation as a cause of ghosts. As noted earlier, no evidence was seen for changes in the line intensities with time, and we have assumed the emission lines to be the same for all of the observing epochs. Following the initial processing of the data, a few ghosts remained that were attributable to particular scans involving the very strongest lines in the observed spectrum. The small frequency sections where these occurred have been reprocessed with the appropriate scans removed. The redundancy of the observations allowed this to be done without significantly increasing the noise present in those sections, and the resulting SSB spectrum is consistent with the DSB observations.

2.3. *Line Identification*

A revised version of the JPL line catalog (Poynter & Pickett 1985) and a catalog provided by F. J. Lovas (1984, private communication) were first used to identify the observed lines. A program written by one of the authors (T.D.G.) and available at the CSO allows the line information from these catalogs to be quickly searched by frequency and species. Relations between line intensities, column densities, and excitation temperatures can also be computed using the line parameters from the JPL catalog within the program. Rotation diagrams may be easily constructed that utilize the values for line strengths and partition functions from the JPL catalog. By specifying a column density and excitation temperature for a set of molecules, together with line profiles, a simulated spectrum may be computed under the assumption of local thermodynamic equilibrium (LTE).

For some species, it was necessary to consult other sources to obtain transition and frequency information. The observed SiCC transitions have been identified using the work of Gottlieb, Vrtílek, & Thaddeus (1989), while the vibrationally excited HCN transitions were identified based on the rotational constants given by De Lucia & Helminger (1977). More accurate frequencies for the SiS transitions were determined using the parameters given by Frum, Engleman, & Bernath (1990).

There remain two unidentified lines in the present data set, out of approximately 45 spectral features (counting blends as a single feature). The rest of the lines have been identified with simple molecules and their isotopomers previously observed in IRC +10216.

2.4. *Data Analysis*

The observed transitions exhibit line profiles characteristic of an expanding shell, whose interpretation is straightforward in terms of optical depths and spatial resolution (Morris 1975; Olofsson et al. 1982). For optically thin lines, flat-topped profiles are seen when the shell is not resolved by the beam whereas double-peaked profiles are observed when the shell is resolved. Optically thick lines exhibit parabolic profiles. We have performed fits to the observed line profiles; the integrated intensities found in this way agreed to within a few percent with the values found by summing over channels out to zero intensity. The integrated intensities presented here are those found by direct summation. In some cases, severe blending of the lines prevented an accurate determination of the intensities of the individual features so that only rough estimates are reported.

In most cases, only one or two lines from a given species occur within the range of our survey. To derive abundance and excitation information, we have therefore combined our results with previously published observations of lower frequency transitions of the same species using the rotation diagram technique. This technique works under the assumptions that the populations of the different molecular levels may be described by a single rotational temperature $T_{\rm rot}$, and that this

temperature is much larger than the background brightness temperature. For an optically thin transition, integrating the equations of radiative transfer yields a relationship between the energy of the upper level and the integrated line intensity which may be written:

$$\frac{3kW}{8\pi^3\nu\mu^2 S} = \frac{N_u}{g_u} = \frac{N_T}{Q(T_{\rm rot})} e^{-E_u/T_{\rm rot}}, \quad (1)$$

where $W = \int T_{\rm MB} dv$ is the integrated intensity, μ is the appropriate component of the dipole moment, S is the line strength, N_T is the column density, Q is the rotational partition function, and E_u is the upper state energy. We have used the partition function and line strength information from the JPL line catalog to ensure that consistently defined state degeneracies and line strengths are used throughout the computations.

The observed line profiles allow us to verify that the transitions used in constructing the rotation diagrams are optically thin. It is clear that the assumption that a single rotational temperature describes the excitation of the molecules will generally not be met, given the source structure of IRC +10216. In general, the more highly excited levels will be preferentially populated in the warmest regions nearest the star, whereas levels of low excitation will be populated over a more extended region. In addition, CO, with its low dipole moment, is the only molecule likely to be completely thermalized by collisions; other molecules are excited to higher vibrational states by the intense infrared radiation field with the subsequent decay back to the ground vibrational state leaving the molecule in an excited rotational level (Morris 1975). Nevertheless, the rotation diagram technique provides useful abundance and excitation information averaged over the beam size and allows comparisons between different species to be made using data which have been processed in the same manner.

We have used observations presented by Kahane et al. (1988, hereafter K1) from the IRAM survey where possible for consistency. Lower frequency transitions (from 87 to 146 GHz) of CS, SiS, SiO, HCN, and CCH as well as isotopically substituted variants of these molecules are included in this data set. We also use the similar observations of CO and ^{13}CO reported by Kahane et al. (1992, hereafter K2). Main beam brightness temperatures were used throughout for the rotation diagram analysis. Without a detailed knowledge of the spatial distribution of the different molecules, accurate corrections for different beam sizes cannot be made. Combining observations with similar beam sizes and efficiencies is therefore essential to obtaining meaningful results. We use their reported intensities with no corrections while noting that this may add to the uncertainties in the derived values. The IRAM beam size and efficiency is not specified in K1 and K2, but Cernicharo et al. (1991) give the respective values as 24″ and 0.65 at 90 GHz and 17″ and 0.60 at 140 GHz. We also adopt the values for isotopic abundances from K1 and K2. Results of other authors used in the analysis are presented in the discussion of individual species.

3. RESULTS AND DISCUSSION

The single-sideband spectrum of IRC +10216 obtained from our survey is plotted in Figure 1, with the strongest lines shown separately in Figure 2. In general, the higher sensitivity and increased spectral resolution relative to the survey of Avery et al. results in clearer detections and observations of the line profiles, particularly for the weaker features. A list of the spectral lines detected in the spectrum is given in Table 2. Again, with the exception of the two unidentified features noted there, the observed lines are identified with molecules that have previously been seen in IRC +10216. In Table 3 we present the integrated intensities of the observed transitions, grouped by species. The derived column densities and rotational temperatures are shown in Table 4, while Table 5 gives the abundances of the different species relative to CO. These values are generally consistent with previous determinations (Johansson et al. 1984; Omont 1987). Further information about the individual species, the specific transitions and intensities is given below.

3.1. *Individual Species*

3.1.1. CO

Our survey includes the $J = 3$–2 transitions of both ^{12}CO and ^{13}CO. The emission from ^{12}CO is optically thick, as is apparent from the observed line shape and from a comparison of the intensities of the lines of the two isotopic variants. The ^{13}CO emission is seen to be optically thin from the doubly peaked line shape, which also indicates that the emission arises from a region that is extended compared to our 20″ beam.

We may derive a column density for the optically thin emission from ^{13}CO in two ways. Taking the brightness temperature (corrected for the Rayleigh-Jeans approximation) of the optically thick and extended emission from ^{12}CO to be the excitation temperature of ^{13}CO, we find that a column density of 4.0×10^{16} cm^{-2} for ^{13}CO is required to produce the observed integrated intensity in the $J = 3$–2 line, with this result varying only slightly as the excitation temperature ranges from 35 to 55 K. We also use the rotation diagram method for the ^{13}CO $J = 3$–2 line from our data and the $J = 2$–1 and $J = 1$–0 lines from K2. In this way we derive a column density of 5.0×10^{16} cm^{-2} and a rotation temperature of 17 K. The somewhat lower temperature is not surprising, since it is computed using states of lower excitation that are likely to have greater populations in cooler regions.

Scaling the ^{13}CO results by 44, the [^{12}C]/[^{13}C] ratio in IRC +10216 found by K2, we obtain column densities for ^{12}CO of 1.8×10^{18} or 2.2×10^{18} cm^{-2} depending on the method used. We adopt a value of 2.0×10^{18} cm^{-2} for use in determining the relative abundances of other species.

This value is in general agreement with previous determinations of the CO abundance. Using an inverse-square law for the molecular density $n = n_0(R_0/r)^2$, Olofsson et al. (1982) give molecular abundances in terms of $n_0R_0^2$ with the range of r for each molecule determined by on- and off-source observations. Converting their results to column density of CO in a 20″ beam yields a value of 1.4×10^{18} cm^{-2}. The mass-loss rate and CO abundance from the Kwan & Linke (1982) model for IRC +10216 yield a value of 3×10^{18} cm^{-2} for the CO column density when converted in a similar manner. Despite its simplifying assumptions, the rotation diagram analysis therefore appears to provide molecular abundance estimates which are consistent with more detailed modeling.

3.1.2. CS

The J = 7–6 transition of CS shows the parabolic shape associated with an optically thick line while the $C^{34}S$ transition is observed to have a flat profile indicating a low optical depth. The $C^{33}S$ J = 7–6 line is heavily blended with the CN $3_{5/2}$–$2_{3/2}$ lines but also appears to have a flat profile. The column density and excitation temperature for $C^{34}S$ shown in Table 4 are derived from a rotation diagram using our 7–6 integrated intensity together with the intensities reported by K1 for the 3–2 and 2–1 lines. For $C^{33}S$, the estimated intensity from this survey and the 2–1 line reported by K1 yield an excitation temperature that is nearly identical to that of $C^{34}S$. However, both the temperature and the derived column density of $C^{33}S$ are significantly more uncertain than the $C^{34}S$ values. To obtain the column density for CS, we therefore scale the $C^{34}S$ value by the $[^{34}S]/[^{32}S]$ ratio of 20.2 from K1. The resulting CS abundance relative to CO of 1.5×10^{-3} falls midway between the values of 7×10^{-4} found by Johansson et al. (1984) with a beam size of 38″ and 3×10^{-3} found by Williams & White (1992, hereafter WW) with a 15″ beam. It seems likely that the CS emission arises from a more compact region than the CO emission causing the CS/CO abundance to appear to increase as the beam size decreases. This is also consistent with the flat-topped profiles detected for $C^{34}S$ and $C^{33}S$ which suggest that our beam does not resolve the emission region.

Our survey also marginally detects emission from CS in the first vibrationally excited state. The J = 5–4 and J = 2–1 transitions of CS in its v = 1 state were originally detected by Turner in IRC +10216 (1987a). A separate observation of the v = 1, J = 7–6 transition detected here was made by Walker, Groesbeck, & Blake (1994) with the CSO and will be presented elsewhere.

3.1.3. HCN

Our survey includes the $HC^{15}N$ J = 4–3 line as well as the J = 4–3 lines from HCN and $H^{13}CN$ reported by WW and Avery et al. The HCN J = 1–0 line has approximately the same intensity as the CO J = 1–0 line, as measured at Onsala (Olofsson et al. 1982; Johansson et al. 1984) and IRAM (K1, K2). With the smaller beam of the JCMT, WW find the HCN J = 4–3 line to be significantly stronger than the CO J = 3–2 line and explain the lower frequency results as the effect of beam dilution for HCN which has a much more compact distribution than CO. However, Avery et al. report a lower intensity for the HCN line than for the CO line. We find the HCN J = 4–3 line to have approximately the same strength as the CO J = 3–2 line, with the line profiles for HCN and its isotopomers consistent with a compact distribution.

The Onsala and IRAM observations as well as the current CSO observations clearly exhibit parabolic line shapes indicative of large optical depths for both HCN and $H^{13}CN$, with the $H^{13}CN$ lines having a strength roughly half that of the HCN lines. The intensity of the $H^{13}CN$ J = 4–3 line reported by WW appears to be too low when compared with the current results. Their HCN J = 4–3 intensity is stronger than ours, consistent with emission from a compact source, but their $H^{13}CN$ intensity is actually weaker than ours by a factor of 4.

Since both HCN and $H^{13}CN$ are optically thick, we use the $HC^{15}N$ J = 4–3 line from this work and the J = 1–0 line from K1 to derive the rotational temperature and column density shown in Table 4. The $[^{14}N]/[^{15}N]$ ratio in IRC +10216 is quite uncertain: estimates for this ratio may be obtained by comparing the $H^{13}CN$ and $HC^{15}N$ emission. These should be regarded as lower limits because of the significant opacity of the $H^{13}CN$ emission. From our integrated intensities, and assuming a $[^{12}C]/[^{13}C]$ ratio of 44, we derive a $[^{14}N]/[^{15}N]$ ratio of >2700, while K1 derive a value of greater than 4400. We use values of 4000 for the $[^{14}N]/[^{15}N]$ ratio and 44 for the $[^{12}C]/[^{13}C]$ ratio to scale our $HC^{15}N$ column density to obtain the column densities shown in Table 4 for HCN and $H^{13}CN$.

We also observe a number of transitions of HCN in vibrationally excited states as shown in Table 3. Ziurys & Turner (1986) first observed emission from the J = 3–2 lines in the excited (0, 1^{1c}, 0), (0, 1^{1d}, 0), and (0, 2^0, 0) levels. Emission from the J = 2–1 and 3–2 lines in all of the (0, 0, 0), (0, 1^1, 0), (0, 2^2, 0), and (0, 2^0, 0) states was reported by Lucas & Cernicharo (1989), with the (0, 1^{1c}, 0) J = 2–1 line exhibiting strong maser emission. Interferometer observations of the J = 1–0 line in the (0, 2^0, 0) state showed evidence of weak maser emission, and the emission region was found to be ~1″ in diameter (Lucas & Guilloteau 1992). Avery et al. reported emission from the J = 4–3 and 3–2 lines in the (0, 1^{1c}, 0), (0, 1^{1d}, 0) levels. We detect emission from the J = 4–3 lines in all of the above states as well as in the (0, 0^0, 1) and (1, 0^0, 0) states. To our knowledge, these represent the highest excitation rotational lines yet seen in this source. There is a general tendency for the lines from vibrationally excited states of HCN to be more triangular than parabolic or flat. This is also true for the lines from vibrationally excited states of other species in IRC +10216. Since these states are almost certainly excited by the intense IR radiation field near the star, the emission regions should generally be very compact. The line shapes may result from peculiar excitation effects or may indicate that the molecules in the vibrational states have not yet reached the terminal outflow velocity (cf. the discussion of vibrationally excited SiS below).

We have tentatively detected the J = 4–3 line of $H^{13}CN$ in the (0, 1^{1c}, 0) level, although the corresponding line of the (0, 1^{1d}, 0) level at 346956.8 MHz which should be equally strong is not clearly seen. However, the detection by Lucas & Cernicharo (1989) of the J = 2–1 line of HCN in the (0, 1^{1c}, 0) level as a 400 Jy maser (brighter than the ground state) in IRC +10216 suggests the possibility of unusual excitation for the (0, 1^{1c}, 0) state of HCN and its isotopomers. In the present survey, we also find rather different line shapes for the J = 4–3 lines of HCN in the (0, 1^{1c}, 0) and (0, 1^{1d}, 0) states.

3.1.4. SiO

The J = 8–7 lines of SiO, ^{29}SiO, and ^{30}SiO lie within the frequency range covered by our survey. The SiO line possesses a somewhat flattened parabolic profile and appears to have at least a moderate optical depth while the ^{29}SiO line exhibits a flat top. Unfortunately, the ^{30}SiO line falls within one of the sections of high noise noted earlier, making an accurate determination of the profile impossible despite the clear detection of the line. The integrated intensities are used in all three cases in conjunction with the J = 2–1 lines observed by K1 to derive rotational temperatures and column densities. K1 find the ratios $[^{28}Si]/[^{29}Si]$ and $[^{28}Si]/[^{30}Si]$ to be relatively unchanged

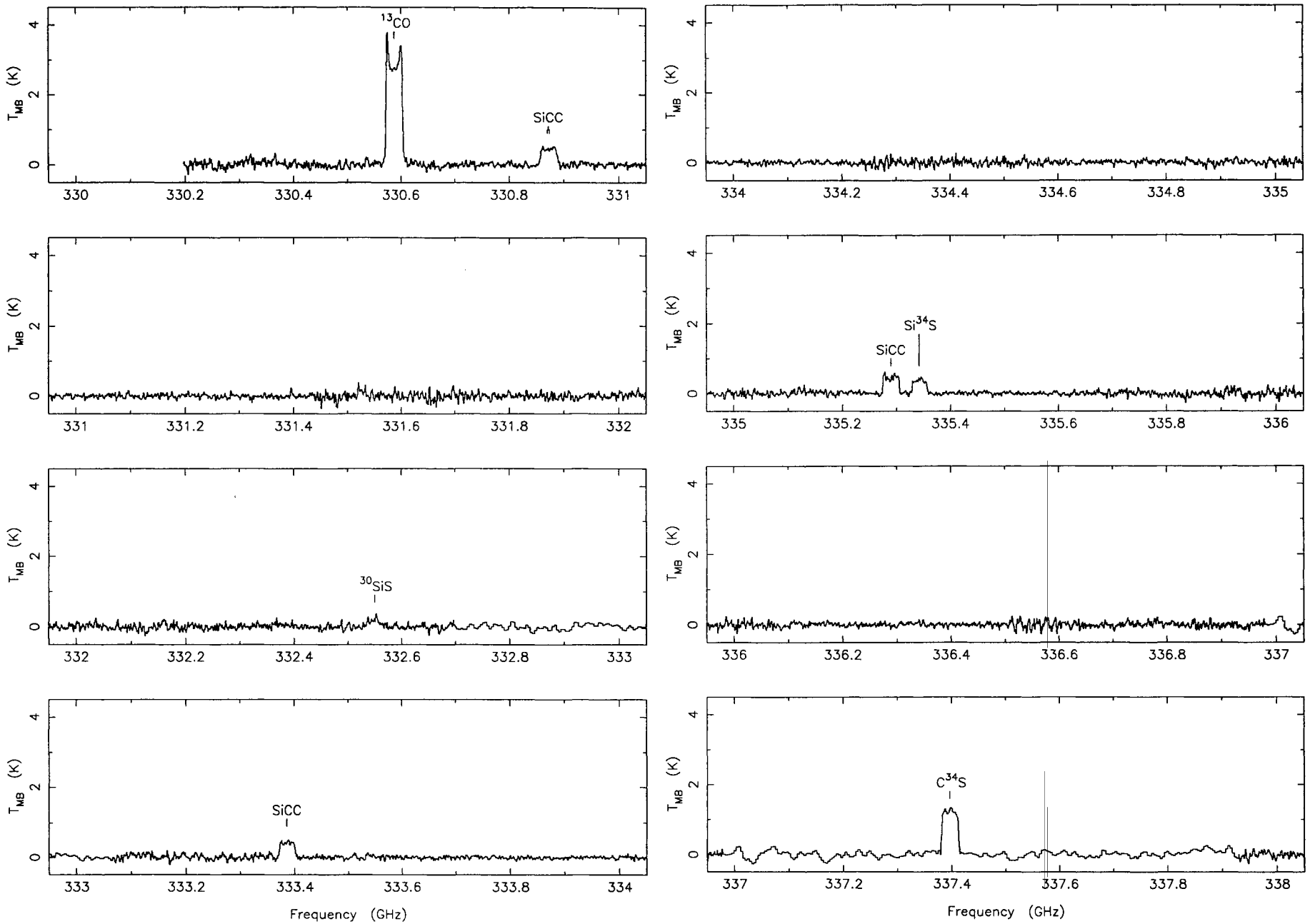

FIG. 1.—Spectrum of IRC +10216 from 330 to 358 GHz. The data have been corrected by the main beam efficiency of 0.60. The rest frequency scale has been established using a v_{LSR} of −26 km s^{-1}. Tick marks show the rest frequencies of identified transitions.

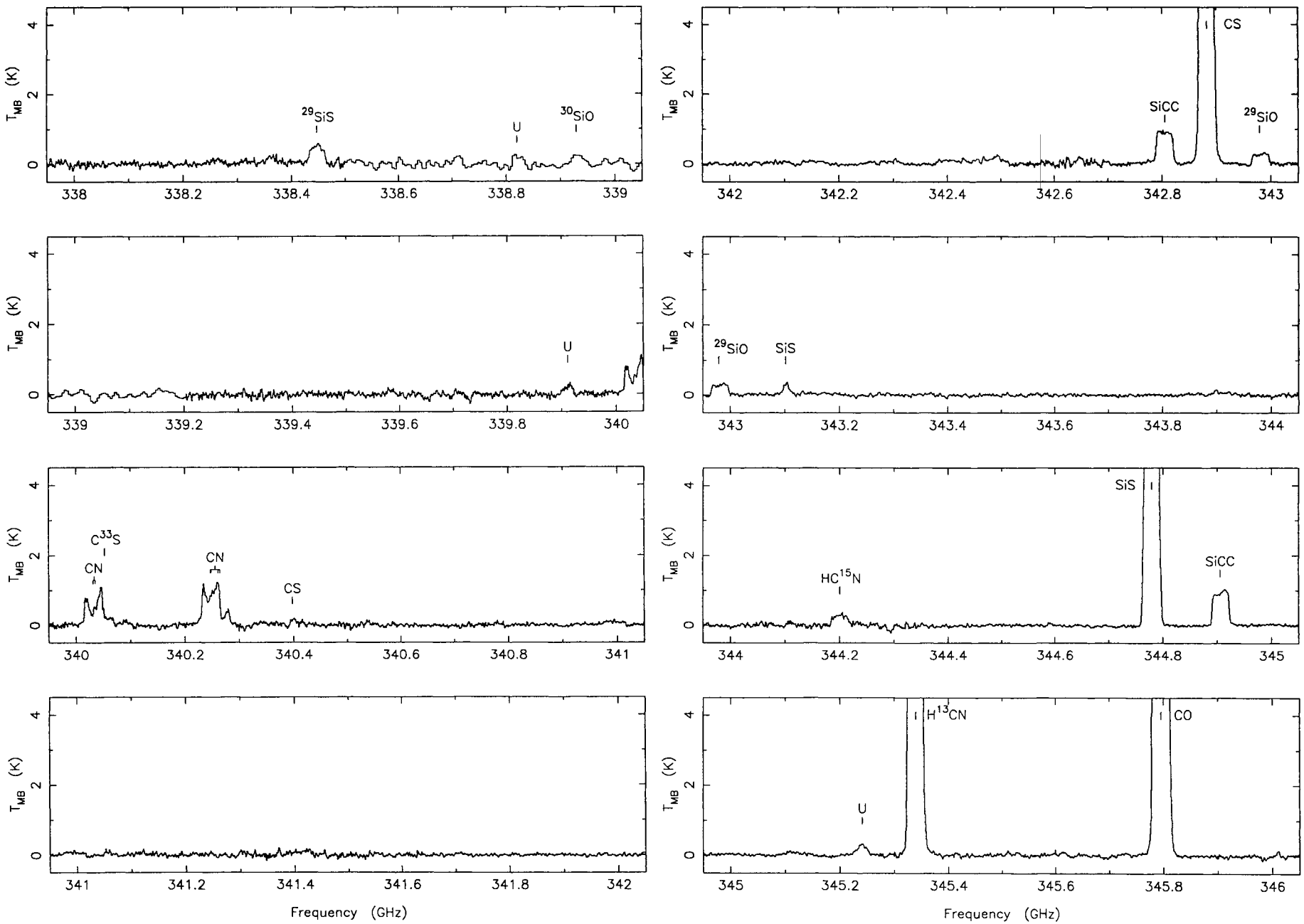

FIG. 1—*Continued*

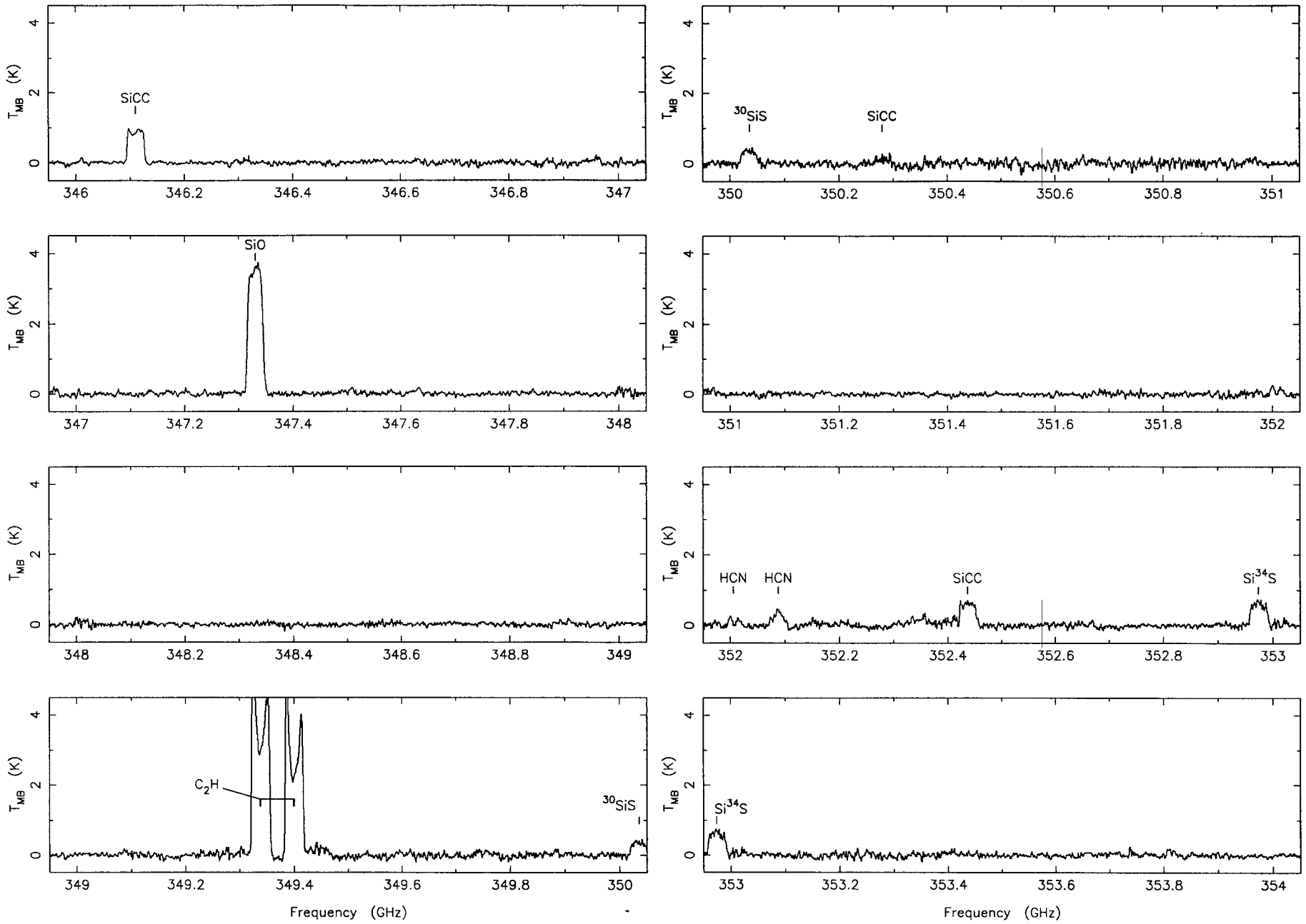

FIG. 1—*Continued*

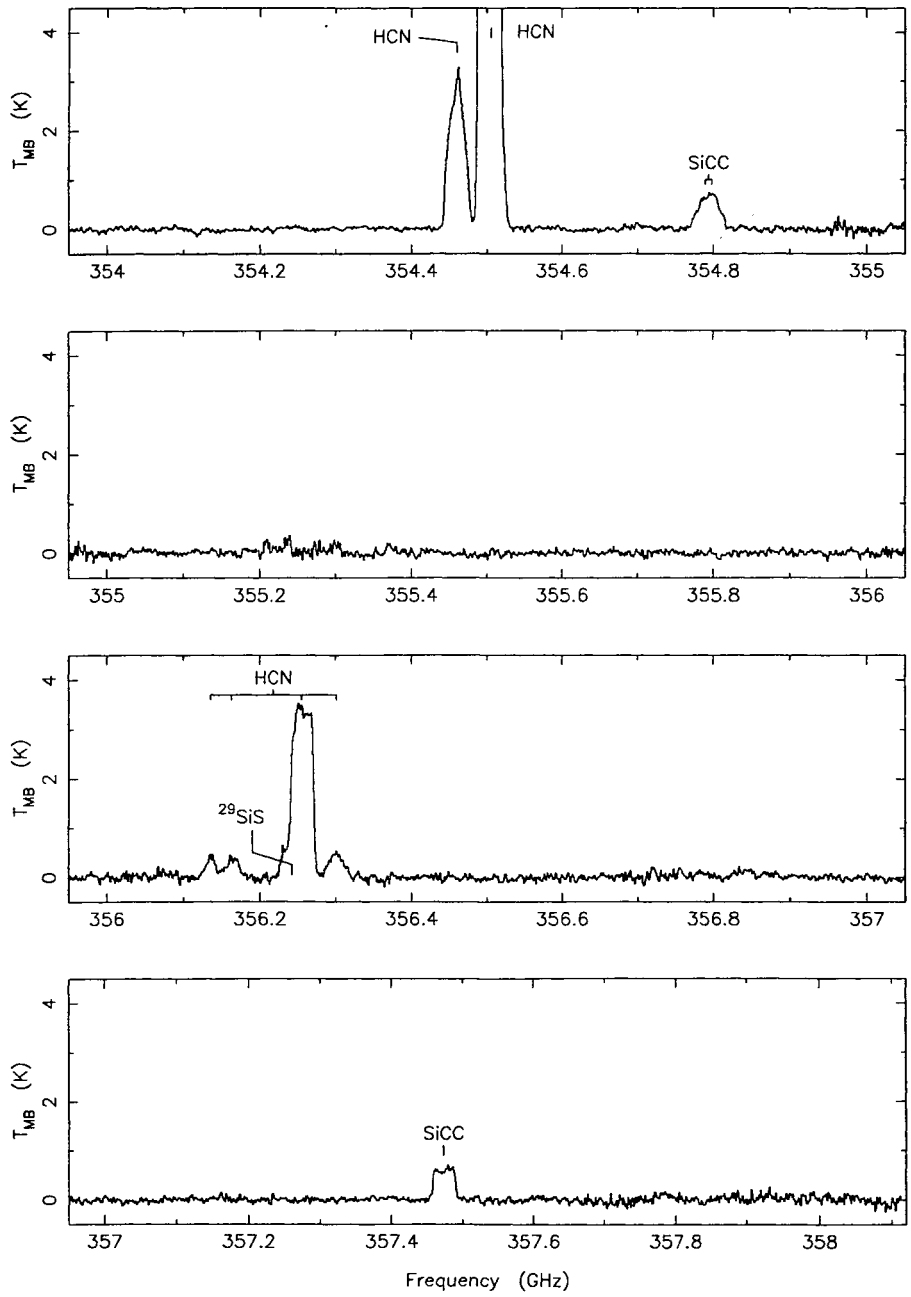

FIG. 1—*Continued*

from their interstellar medium (ISM) values. Scaling our ^{29}SiO and ^{30}SiO results by the ratios from K1 yields values for the SiO column density greater by ~65% than the value derived directly from the SiO intensities, again suggesting a moderate optical depth in the parent SiO lines.

3.1.5. SiS

We observe a total of seven lines from SiS, ^{29}SiS, ^{30}SiS, and Si^{34}S in our survey. The J = 19–18 line is detected for all four isotopomers, while the J = 20–19 line is seen in the three heavier variants (the line for SiS occurs at 362.9 GHz, outside the observed frequency range). Of these lines, the ^{29}SiS J = 20–19 line is severely blended with the HCN (0, 1^{1d}, 0) J = 4–3 line, and the ^{30}SiS J = 19–18 is detected at a lower signal-to-noise ratio, making determination of the profiles difficult. The remaining lines exhibit profiles consistent with previous interferometer observations showing the J = 5–4 and J = 6–5 SiS emission to be strongly peaked at the location of the star with a rapid falloff with radial distance (Beiging & Nguyen-Q-Rieu 1989). The compact nature of the emission and additional observations of the J = 4–3 and J = 6–5 SiS lines showing profiles with no central dip (Johansson et al. 1984) indicate that the J = 5–4 profile with "horns" at the extreme velocities (Olofsson et

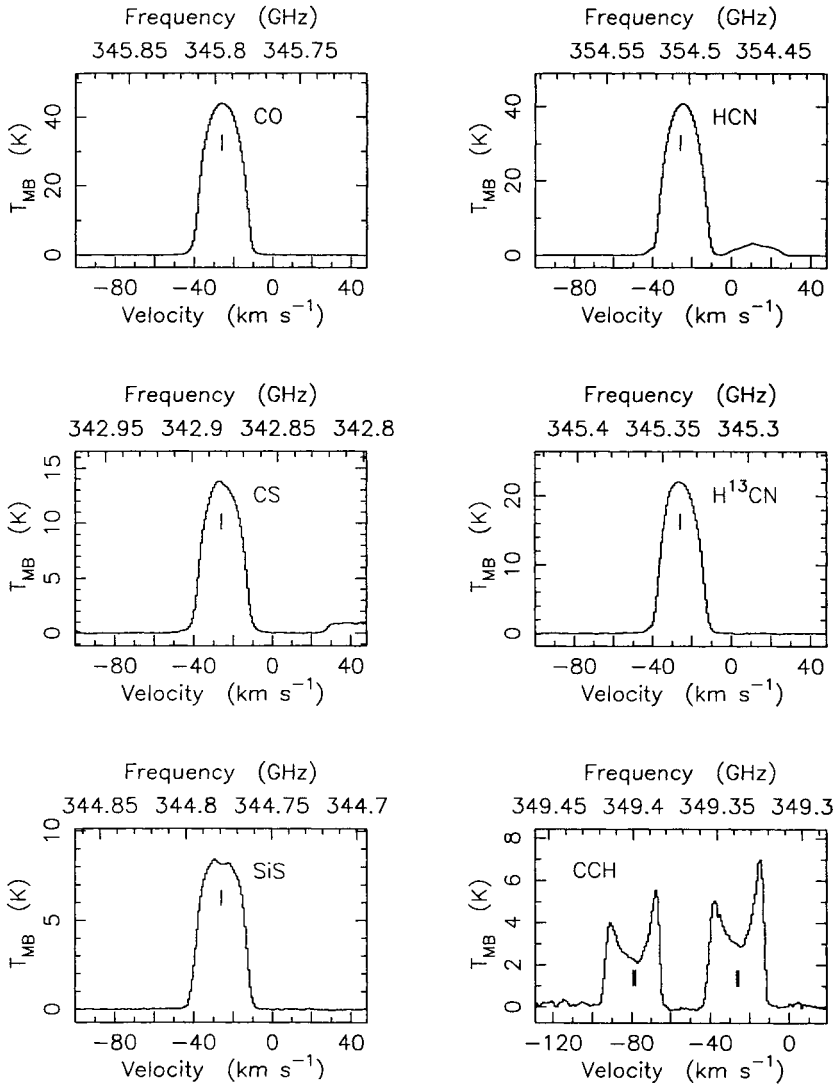

FIG. 2.—Strong lines observed within the frequency range covered by the survey. Tick marks indicate the rest frequencies of the lines and are shown at −26 km s^{-1} for all lines except the CCH blends. For these, the reference velocity of −26 km s^{-1} occurs midway between the lower frequency pair of lines. The unlabeled weaker lines which are visible are from SiCC at 342.805 GHz and from the vibrationally excited HCN (0, 1^{1c}, 0) state at 354.460 GHz.

al. 1982; Johansson et al. 1984; K1; Bieging & Nguyen-Q-Rieu 1989) results from peculiar excitation effects rather than from resolved optically thin emission. We perform the rotation diagram analysis using our observed lines and the $J = 8$–7 and $J = 5$–4 lines from K1 for SiS and its isotopomers. The resulting temperatures are distinctly higher than those found for other species, consistent with a location closer to the central star. Scaling the results for ^{29}SiS, ^{30}SiS, and Si^{34}S by the isotope ratios of K1 gives consistent values for the SiS column density which are only ~25% larger than the results obtained using the SiS lines themselves. Avery et al. combine a number of previous SiS observations at lower frequencies with the $J = 20$–19 and 19–18 lines from their survey and derive a column density of 6.5×10^{15} cm^{-2} and a temperature of 53 K. Their somewhat higher column density and lower temperature relative to our beam-averaged values most likely result from the source size of 15″ assumed in their analysis.

We additionally detect the $J = 19$–18 transition of SiS in the $v = 1$ vibrationally excited state with a triangular line profile similar to the vibrationally excited HCN lines. Guélin et al. (1987) have reported the $J = 9$–8 transition of SiS in this state, while Turner (1987b) detects the $J = 12$–11, 13–12, and 14–13 transitions. The line profiles for these other transitions are similar to ours, with Turner suggesting that the SiS $v = 1$ emission arises from a very compact region within the accelerating zone.

3.1.6. SiCC

A total of 14 transitions of SiCC are detected in our survey, with some of these blended together so that ten resolved spectral features are observed. The energies of the states involved in these transitions range from 130 to 330 K, with $J_{upper} = 14$, 15, and 16. Figure 3 shows the rotation diagram for the present data set which yields a rotational temperature of 106 K and a column density of 3.7×10^{14} cm^{-2}. Thaddeus et al. (1984), with a beam size of 90″, originally found different excitation

TABLE 2

LINES DETECTED IN THE CSO SPECTRAL LINE SURVEY OF IRC +10216

Frequency (MHz)	Species	Transition	Frequency (MHz)	Species	Transition
330588.1	^{13}CO	3 – 2	344906.0	SiCC	$16_{0,16} - 15_{0,15}$
330870.5	SiCC	$14_{6,9} - 13_{6,8}$	345238.7	$H^{13}CN$ (0,1^{1c},0) [a]	4 – 3
330874.5	SiCC	$14_{6,8} - 13_{6,7}$	345339.8	$H^{13}CN$	4 – 3
332550.3	^{30}SiS	19 – 18	345796.0	CO	3 – 2
333386.1	SiCC	$14_{4,11} - 13_{4,10}$	346110.0	SiCC	$14_{2,12} - 13_{2,11}$
335289.7	SiCC	$14_{4,10} - 13_{4,9}$	347330.6	SiO	8 – 7
335342.0	$Si^{34}S$	19 – 18	349337.5	C_2H	$4,\frac{9}{2},5 - 3,\frac{7}{2},4$
337396.7	$C^{34}S$	7 – 6	349338.7	C_2H	$4,\frac{9}{2},4 - 3,\frac{7}{2},3$
338447.3	^{29}SiS	19 – 18	349398.9	C_2H	$4,\frac{7}{2},4 - 3,\frac{5}{2},3$
338821	U		349400.3	C_2H	$4,\frac{7}{2},3 - 3,\frac{5}{2},2$
338929.0	^{30}SiO	8 – 7	350035.7	^{30}SiS	20 – 19
339911	U		350280.0	SiCC	$15_{10,5} - 14_{10,4}$
340031.5	CN	$3,\frac{5}{2},\frac{7}{2} - 2,\frac{3}{2},\frac{5}{2}$	350280.0	SiCC	$15_{10,6} - 14_{10,5}$
340035.4	CN	$3,\frac{5}{2},\frac{3}{2} - 2,\frac{3}{2},\frac{1}{2}$	352005.7	HCN (0,0^0,1)	4 – 3
340035.4	CN	$3,\frac{5}{2},\frac{5}{2} - 2,\frac{3}{2},\frac{3}{2}$	352087.9	HCN (1,0^0,0)	4 – 3
340052.7	$C^{33}S$	7 – 6	352436.5	SiCC	$15_{8,8} - 14_{8,7}$
340247.8	CN	$3,\frac{7}{2},\frac{7}{2} - 2,\frac{5}{2},\frac{5}{2}$	352436.5	SiCC	$15_{8,7} - 14_{8,6}$
340247.8	CN	$3,\frac{7}{2},\frac{9}{2} - 2,\frac{5}{2},\frac{7}{2}$	352974.0	$Si^{34}S$	20 – 19
340248.6	CN	$3,\frac{7}{2},\frac{5}{2} - 2,\frac{5}{2},\frac{3}{2}$	354460.3	HCN (0,1^{1c},0)	4 – 3
340261.8	CN [a]	$3,\frac{7}{2},\frac{3}{2} - 2,\frac{5}{2},\frac{1}{2}$	354505.5	HCN	4 – 3
340265.0	CN [a]	$3,\frac{7}{2},\frac{7}{2} - 2,\frac{5}{2},\frac{7}{2}$	354789.5	SiCC	$15_{6,10} - 14_{6,9}$
340398.1	CS (v=1)	7 – 6	354798.4	SiCC	$15_{6,9} - 14_{6,8}$
342805.0	SiCC	$15_{2,14} - 14_{2,13}$	356135.4	HCN (0,2^{2d},0)	4 – 3
342883.0	CS	7 – 6	356162.7	HCN (0,2^{2c},0)	4 – 3
342979.1	^{29}SiO	8 – 7	356242.4	^{29}SiS	20 – 19
343101.0	SiS (v=1)	19 – 18	356255.7	HCN (0,1^{1d},0)	4 – 3
344200.3	$HC^{15}N$	4 – 3	356301.3	HCN (0,2^0,0)	4 – 3
344779.5	SiS	19 – 18	357473.4	SiCC	$15_{4,12} - 14_{4,11}$

[a] Tentative identification. See discussion of individual species.

temperatures for transitions within and across the K_a ladders. Since the odd K_a states are missing, cross-ladder transitions corresponding to $\Delta K_a = 2$ are only weakly allowed. Thaddeus et al. suggested the warm cross-ladder temperature of 140 K is controlled by collisions while the rapid radiative decay within a given K_a ladder gives a much lower (10 K) rotational temperature for transitions within the same ladder. Avery et al. find evidence for both warm (60 K) and cool (14 K) gas within the ladders, with a cross-ladder temperature of 180 K. They suggest that infrared excitation rather than collisions is responsible for the observed high excitation. Cernicharo et al. (1991) derived a single rotational temperature of ~30 K using many of the same lines as Thaddeus, but with a beam size of ~25″. Similarly, we do not find evidence for different temperatures, but note that the narrow (and rather high) range of J values observed by us do not provide a good measurement of the temperature within a single ladder. Our derived column density is significantly lower than that of Avery et al., in large part because of the difference between the derived excitation temperatures.

3.1.7. CN

The CN (N = 3–2) lines lie in the frequency range of our survey. Three of the hyperfine transitions occur in a blend at ~340035 MHz, with the line profile showing pronounced horns indicative of low optical depth and extended emission. A second blend of three hyperfine transitions occurs at ~340248 MHz, again with pronounced horns, but also blended with another feature. We have tentatively assigned this second feature to a blend of two more hyperfine transitions of CN at ~340263 MHz, but we note that the intensity of this last feature is much larger relative to that of the other blends than expected from LTE calculations.

Avery et al. report detections of all of the hyperfine lines, noting that they are blended. The improved sensitivity of our survey makes it clear which of the transitions are actually seen, although some of the blending remains. Where necessary, we assign intensities to the individual transitions based on the relative LTE line strengths. The observed intensities (including transitions not detected) are consistent with these strengths except for the highest frequency blend noted above.

For the rotation diagram, we use the N = 2–1 lines observed by Wootten et al. (1982) with a 30″ beam at OVRO and the N = 1–0 lines observed by Truong-Bach et al. (1987) with a 34″ beam at Onsala. CN was seen by them to exist in an extended shell, consistent with its likely derivation as the photodissociation product of HCN. We derive a low rotation temperature, which in turn results in a significantly lower column density than that estimated from the earlier lower frequency observations but in good agreement with the results of Avery et al..

3.1.8. CCH

CCH is also a photodissociation product (of C_2H_2), and its distribution as deduced from interferometer maps as well as single-dish observations is a shell-like structure with a radius of ~15″ (Lucas 1992; Bieging & Nguyen-Q-Rieu 1988; Truong-

TABLE 3

TRANSITION ENERGIES AND INTEGRATED INTENSITIES

Species	Frequency (MHz)	Transition	E_{lower} (K)	$\int T_{MB}\,dv$ (K km s^{-1})
CO	345796.0	3 – 2	16.6	955.6
^{13}CO	330588.1	3 – 2	15.9	86.4
CS	342883.0	7 – 6	49.4	301.5
CS (v=1)	340398.1	7 – 6	1879.4	2.0
C^{34}S	337396.7	7 – 6	48.6	34.2
C^{33}S	340052.7	7 – 6	49.0	~3 [a]
SiO	347330.6	8 – 7	58.3	87.8
^{29}SiO	342979.1	8 – 7	57.6	8.0
^{30}SiO	338929.0	8 – 7	56.9	4.5
SiS	344779.5	19 – 18	149.0	201.7
SiS (v=1)	343101.0	19 – 18	1219.4	4.3
^{29}SiS	338447.3	19 – 18	146.2	13.5
	356242.4	20 – 19	162.5	~20 [b]
^{30}SiS	332550.3	19 – 18	143.7	5.1
	350035.7	20 – 19	159.6	8.4
Si^{34}S	335342.0	19 – 18	144.9	9.6
	352974.0	20 – 19	161.0	17.2
CN	340031.5	$3,\frac{5}{2},\frac{7}{2} - 2,\frac{3}{2},\frac{5}{2}$	16.3	~21 [c]
	340035.4	$3,\frac{5}{2},\frac{3}{2} - 2,\frac{3}{2},\frac{1}{2}$	16.3	...
	340035.4	$3,\frac{5}{2},\frac{5}{2} - 2,\frac{3}{2},\frac{3}{2}$	16.3	...
	340247.8	$3,\frac{7}{2},\frac{7}{2} - 2,\frac{5}{2},\frac{5}{2}$	16.3	34.5 [d]
	340247.8	$3,\frac{7}{2},\frac{9}{2} - 2,\frac{5}{2},\frac{7}{2}$	16.3	...
	340248.6	$3,\frac{7}{2},\frac{5}{2} - 2,\frac{5}{2},\frac{3}{2}$	16.3	...
	340261.8	$3,\frac{7}{2},\frac{5}{2} - 2,\frac{5}{2},\frac{5}{2}$	16.3	...
	340265.0	$3,\frac{7}{2},\frac{7}{2} - 2,\frac{5}{2},\frac{7}{2}$	16.3	...
HCN	354505.5	4 – 3	25.5	831.7
HCN (0,1^{1c},0)	354460.3	4 – 3	1050 [e]	62.5
HCN (0,1^{1d},0)	356255.7	4 – 3	1050 [e]	~72 [f]
HCN (0,2^{0},0)	356301.3	4 – 3	2056 [e]	9.4
HCN (0,2^{2c},0)	356162.7	4 – 3	2078 [e]	6.3 [g]
HCN (0,2^{2d},0)	356135.4	4 – 3	2078 [e]	5.2 [g]
HCN (0,0^{0},1)	352005.7	4 – 3	3042 [e]	2.6
HCN (1,0^{0},0)	352087.9	4 – 3	4789 [e]	6.8
HC^{15}N	344200.3	4 – 3	24.8	7.7
H^{13}CN	345339.8	4 – 3	24.9	450.4
H^{13}CN (0,1^{1c},0)	345238.7	4 – 3	1041 [h]	6.0
C_2H	349337.5	$4,\frac{9}{2},5 - 3,\frac{7}{2},4$	25.1	121.3 [i]
	349338.7	$4,\frac{9}{2},4 - 3,\frac{7}{2},3$	25.1	...
	349398.9	$4,\frac{7}{2},4 - 3,\frac{5}{2},3$	25.2	93.3 [i]
	349400.3	$4,\frac{7}{2},3 - 3,\frac{5}{2},2$	25.2	...
SiCC	330870.5	$14_{6,9} - 13_{6,8}$	173.2	6.4 [j]
	330874.5	$14_{6,8} - 13_{6,7}$	173.2	6.4 [j]
	333386.1	$14_{4,11} - 13_{4,10}$	134.7	11.0
	335289.7	$14_{4,10} - 13_{4,9}$	134.8	13.0
	342805.0	$15_{2,14} - 14_{2,13}$	124.9	26.3
	344906.0	$16_{0,16} - 15_{0,15}$	127.6	27.1
	346110.0	$14_{2,12} - 13_{2,11}$	115.0	24.6
	350280.0	$15_{10,5} - 14_{10,4}$	311.5	1.6 [j]
	350280.0	$15_{10,6} - 14_{10,5}$	311.5	1.6 [j]
	352436.5	$15_{8,8} - 14_{8,7}$	242.9	9.1 [j]
	352436.5	$15_{8,7} - 14_{8,6}$	242.9	9.1 [j]
	354789.5	$15_{6,10} - 14_{6,9}$	189.1	9.5 [j]
	354798.4	$15_{6,9} - 14_{6,8}$	189.1	9.5 [j]
	357473.4	$15_{4,12} - 14_{4,11}$	150.7	16.6
U	338821			3.3
U	339911			3.0

[a] Blended with CN $3_{\frac{5}{2}}$–$2_{\frac{3}{2}}$ lines; intensity is estimated.
[b] Blended with HCN (0, 1^{1d}, 0) line; intensity is estimated.
[c] Blend of CN $3_{\frac{5}{2}}$–$2_{\frac{3}{2}}$ lines and C^{33}S lines; a single intensity is estaimted for the blended CN lines.
[d] Blend of CN $3_{\frac{7}{2}}$–$2_{\frac{5}{2}}$ lines; a single integrated intensity is given for the blended lines.
[e] Taken from Carter et al. 1993.
[f] Blended with ^{29}SiS line; intensity is estimated.
[g] Blended HCN lines; intensity of each is estimated.
[h] Taken from Wang & Overend 1973.
[i] Blends of C_2H lines; a single integrated intensity is given for each blend.
[j] SiCC lines with equal energies and line strengths which are blended together; equal intensities are assigned to each line.

TABLE 4

ROTATION DIAGRAM RESULTS

Species	T_{rot} [a] (K)	N_T (cm^{-2})
^{13}CO	17	5.0×10^{16}
CO	...	2.0×10^{18} [b]
$C^{34}S$	28	1.5×10^{14}
$C^{33}S$	28	1.4×10^{13}
CS	...	3.0×10^{15} [b]
SiO	29	2.1×10^{14}
^{29}SiO	29	1.9×10^{13}
^{30}SiO	28	1.1×10^{13}
SiO	...	3.5×10^{14} [b]
SiS	70	3.0×10^{15}
^{29}SiS	85	2.1×10^{14}
^{30}SiS	66	1.2×10^{14}
$Si^{34}S$	79	1.8×10^{14}
SiS	...	3.8×10^{15} [b]
SiCC	106	3.7×10^{14}
CCH	16	4.6×10^{15}
CN	8.7	6.2×10^{14}
$HC^{15}N$	29.1	6.3×10^{12}
$H^{13}CN$	...	2.8×10^{14} [b]
HCN	...	2.8×10^{16} [b]

[a] T_{rot} is not shown for species whose column density is obtained by scaling.

[b] Column density is obtained by scaling from results for other isotopomers (see text).

Bach et al. 1987). We observe the $N = 4$–3, $J = 9/2$–$7/2$ and $J = 7/2$–$5/2$ lines in our survey, with profiles consistent with a low optical depth and a somewhat extended distribution. Combining our observations with the $N = 1$–0 data of K1, we derive a rotation temperature and a column density which agree well with the values obtained by Avery et al.

3.1.9. *Unidentified Lines*

Two lines remain unidentified in our survey at 338821 and 339911 MHz. Interestingly, neither line appears in the JCMT 870 μm survey while we do not detect any of their unidentified lines in the range of our survey despite the considerably increased sensitivity. No molecular species included in the catalogs listed above appear to be likely candidates for the present unidentified lines. We have also checked the available frequencies of transitions from vibrationally excited states of molecules previously seen in IRC +10216.

TABLE 5

RELATIVE ABUNDANCES IN IRC +10216

Species	$x(i)/x(CO)$
CS	1.5×10^{-3}
SiO	1.8×10^{-4}
SiS	1.9×10^{-3}
SiCC	1.9×10^{-4}
CCH	2.3×10^{-3}
CN	3.1×10^{-4}
HCN	1.4×10^{-2}

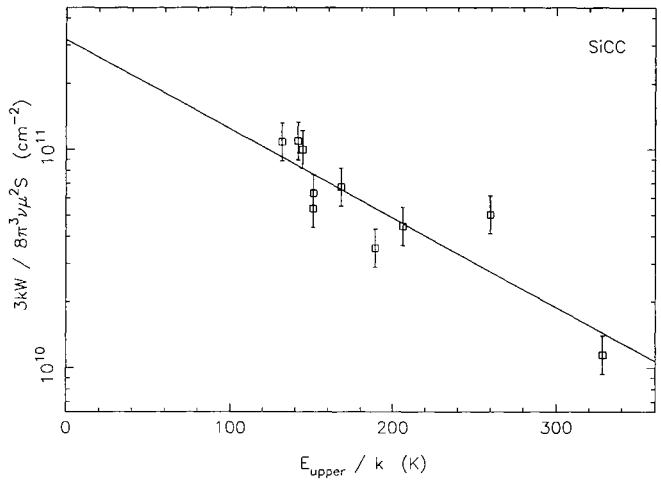

FIG. 3.—Rotation diagram for the SiCC transitions detected in the CSO survey of IRC +10216. Error bars correspond to an estimated uncertainty of 30% in the observed line intensities.

3.2. *Integrated Line Intensity*

Sutton et al. (1984) found that a large fraction of the total millimeter-wave flux from Orion-KL was contained in molecular line emission; this is true at submillimeter wavelengths as well (Groesbeck, Philips, & Blake 1994). Figure 4 displays the spectra from the CSO surveys of Orion-KL and IRC +10216 over the frequency range 330–360 GHz. The relative sparseness of the IRC +10216 spectrum is striking. Despite this, the emission from molecular lines represents a substantial fraction of the total broadband flux at these wavelengths. When averaged over the frequency range of the survey, the lines reported here contribute a flux of 4.9 Jy.

Following Sutton et al. (1984), we estimate the contribution from undetected weak lines by extrapolating the distribution of line intensities to weaker values. Figure 5 shows this distribution as the total number of lines observed which are stronger than a given integrated intensity together with a power-law fit to this distribution of slope −0.6. A somewhat steeper distribution with a slope of −0.8 was found for the Onsala 3 mm survey (Johansson et al. 1984; Avery 1987). For the JCMT 870 μm survey, Avery et al. obtain a rough value of −3/2 for the slope but suggest that this value, which is based on relatively few lines, may be too high. We note, however, that any slope steeper than −1 would in fact yield a diverging (infinite) flux contribution when integrated to lines of zero intensity. To derive the present value of −0.6, we have used the integrated intensities rather than the peak intensities of the lines, with intensities for blended lines split among the different lines according to their LTE values. The resulting fit suggests that an additional 0.4 Jy is contributed by lines which are below our sensitivity limit, giving a total of 5.3 Jy for the line flux.

The total flux density for IRC +10216 at 900 μm has been measured to be 9 Jy by Sopka et al. (1985) in a 47″ beam. As reported by Avery et al., observations at the JCMT by Sandell with an 18″ beam gave a total flux at 850 μm of 4.8–6.5 Jy depending upon the phase of the infrared cycle, while a heterodyne (narrowband) measurement by Sandell at a frequency deliberately chosen to be free of line emission yielded a value of

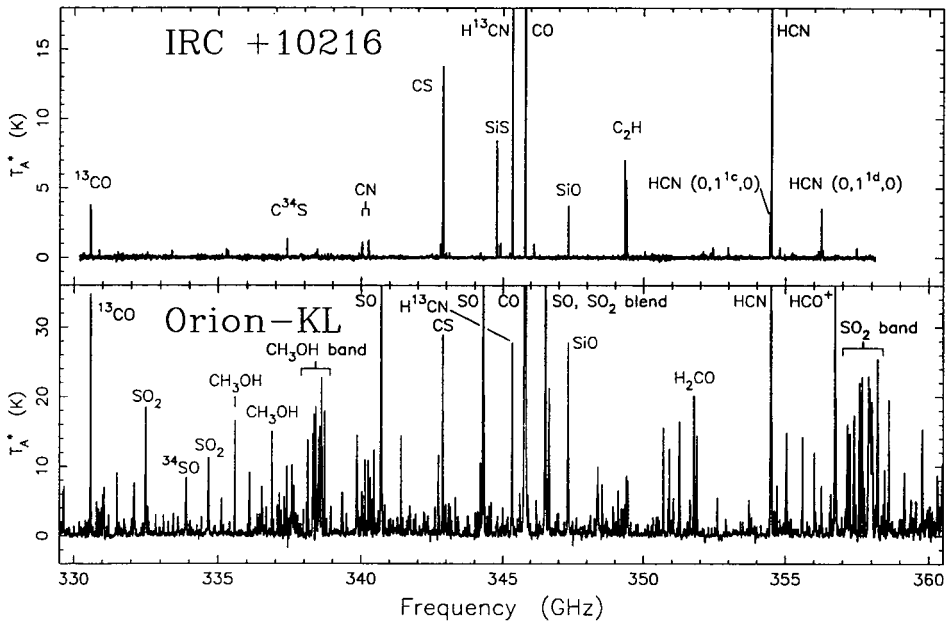

FIG. 4.—Comparison of the CSO spectral line surveys of IRC +10216 and Orion-KL. The data have been corrected by the main beam (0.6) and extended efficiencies (0.76) for IRC +10216 and Orion-KL, respectively. Note the difference in vertical scale between the two panels.

1.9 Jy for the true continuum flux density. Line emission therefore contributes ≳65% to broadband flux measurements of IRC +10216 in the atmospheric window near 345 GHz.

An important question is to what extent the molecular line flux affects measurements of the frequency dependence of the dust emission from IRC +10216. For a grain emissivity which varies as $\sim\lambda^{-\beta}$, the flux from optically thin dust will vary as $S_{\rm dust} \sim \lambda^{-\alpha} \sim \lambda^{-(\beta+2)}$ in the Rayleigh-Jeans limit. Previous observations from 50 to 1000 μm have suggested that the emissivity index β is approximately unity, with a recent fit yielding a value of 1.2 (Campbell et al. 1976; Sopka et al. 1985). The variation of the line emission with frequency is more difficult to estimate. For transitions involving states with energies below the rotational temperature, the flux dependence for the transitions of a linear molecule may range between ν^3 (optically thick) and ν^5 (optically thin), with symmetric and asymmetric top molecules showing even steeper variations (Sutton et al. 1984). At higher frequencies, the line flux will eventually decrease as the level populations decrease with increasing excitation. In addition, the observed flux from a particular molecule will be determined by the precise frequency range included in any measurement and the transition frequencies of the molecule. The actual frequency dependence of line emission will therefore depend in a complicated way on the particular chemistry and physical conditions of the object under study as well as the observing parameters.

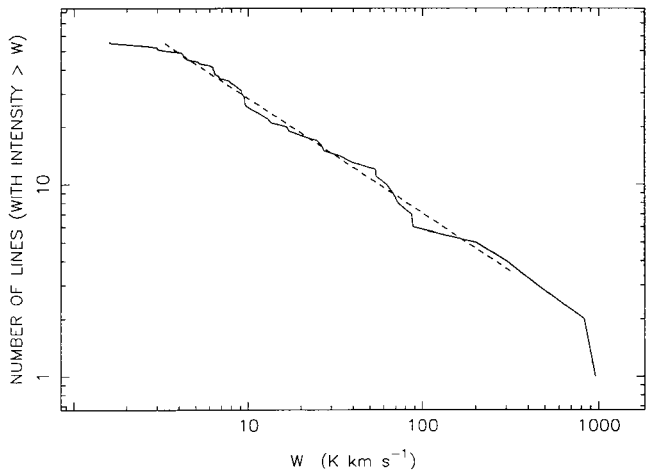

FIG. 5.—Number of lines with integrated intensities greater than W as a function of W for the CSO survey of IRC +10216. The dashed line is a fit to the data over the range $5 < W < 200$ and has a slope of −0.6.

To evaluate this dependence for IRC +10216, we have constructed a simulated spectrum up to 1000 GHz, shown in Figure 6, using the JPL line catalog and the program described earlier. For each species, a column density and temperature, together with a velocity line profile, are used to simulate the lines that would be observed under LTE conditions. We have adopted the column densities and excitation temperatures derived in this paper together with values from Johansson et al. (1984) for HC_3N and HC_5N. This spectrum was originally constructed with a resolution of 1 MHz so that individual lines may be accurately represented. The resulting spectrum is then convolved with a 20 GHz (FWHM) Gaussian and a 100 GHz (FWHM) Gaussian for comparison with the response of broadband instruments to the line flux. The overall appearance of the simulated spectrum results from the emission in strong lines, with the highest peaks resulting when two or more lines lie quite close in frequency. This structure is evidence of the dominance of the few strong lines in determining the actual line flux, as would be expected for a relatively flat line intensity distribution. In the present survey, approximately 80% of the total line flux observed is contributed by the few strong lines shown in Figure 2.

At a lower frequency, Walmsley et al. (1991) have presented

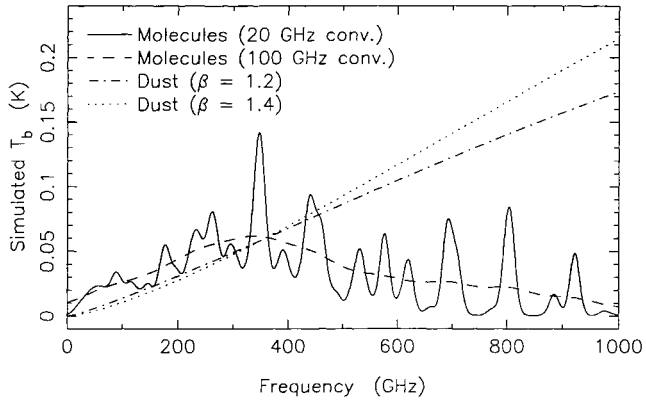

FIG. 6.—Simulated LTE molecular line spectrum of IRC +10216 obtained using the column densities and rotation temperatures from this survey after convolution with a 20 GHz (FWHM) Gaussian and with a 100 GHz Gaussian. Emission corresponding to dust at a temperature of 100 K and scaled to give a flux of 1.9 Jy at 350 GHz is shown for two different values of the emissivity index β. The simulated T_b is equivalent to observations corrected for beam efficiency when the source fills the beam.

continuum measurements made with a 50 GHz bolometer passband. Using estimates of integrated line flux from a 10 GHz section of the IRAM survey near 230 GHz together with a sum of known strong lines, they obtain an estimate of ~0.6 Jy for the contribution of line emission to their total measured flux of ~1.5 Jy. This result may in fact be too low, as several species not listed by them exhibit strong emission in our observations as well as those of K1 and K2. We estimate that including the lines of these species ($H^{13}CN$ J = 3–2 and SiS J = 12–11, 13–12, and 14–13) in their sum of strong lines would increase the line flux to ~0.8 Jy. It would also have the effect of making the emission from strong lines more dominant in determining the total line flux, in agreement with the present observations.

In Figure 6 we have also shown the expected contribution of dust emission, with the value at 350 GHz fixed at 1.9 Jy based upon the heterodyne measurement of Sandell. The dust was taken to have an optical depth of 1 at a wavelength of 10 μm (Sopka et al. 1985) and a temperature of 100 K (Kwan & Linke 1982). We have plotted the emission for two values of the emissivity index: β = 1.2 as derived by Sopka et al. (1985) and β = 1.4 reflecting our conclusion below that the index is likely to increase as a result of corrections for line emission. The dust emission (in T_b units) continues to rise throughout the range shown, while the rollover of the molecular line emission results from the generally cooler gas temperatures.

Previous determinations of the emissivity index in IRC +10216 have generally relied on broadband flux measurements made at wavelengths ranging from the mid- and far-infrared to the submillimeter band. Since line emission may represent a significant fraction of the total flux observed, corrected values representing the flux from the dust should be used in determining the value of β. In practice, however, the amount of the correction needed at different frequencies is not known. The simulated spectra shown in Figure 6 suggest that the correction for line flux will be greatest at the longer wavelengths. The line flux corrections are likely to be relatively unimportant at mid- and far-infrared wavelengths, so that these measurements constrain the overall fit and will limit any change in the value of β to be fairly small. The present spectral survey and our simulations of the line emission contribution indicate that substantial corrections to broadband flux measurements are needed in the submillimeter range. When applied, these corrections bring the emissivity index as determined from the longer wavelength measurements alone into better agreement with the value resulting from the entire wavelength range.

Using published observations of the total flux from IRC +10216 at wavelengths ranging from 50 to 1000 μm together with their own observations at 400, 450, and 900 μm, Sopka et al. (1985) derive a value of 1.2 for β. Using the reported flux values at 450 and 900 μm, we obtain a value of 1.7 for α, or approximately 0 for β. If we instead correct the flux values for an estimated line flux contribution of 15% at 450 μm and 65% at 900 μm, we derive a value of 3.0 for α or 1.0 for β, in better agreement with the overall fit. Similar results are obtained from observations at 450 μm and 850 μm by G. H. L. Sandell (1992, private communication), for which the uncorrected total flux values yield α = 1.9, suggesting optically thick emission even at 850 μm. Using the same corrections for the line flux contribution, we instead obtain a value of 3.3 for α, a value which agrees well with that obtained from fits over the entire range from mid-infrared to submillimeter wavelengths. Additional measurements of the total flux at 1.1 and 1.3 mm by Sandell also appear to require substantial corrections for the presence of line emission to be consistent with $\beta \sim 1$. This agrees with the results of our simulations indicating that the integrated line flux may represent $\gtrsim$50% of the total flux at wavelengths longer than ~750 μm.

Thus, receivers with narrow frequency response functions chosen to avoid regions of significant line emission must be used to make true continuum measurements. As an alternative, the line emission contribution to broadband flux measurements could be modeled using simulated line spectra similar to the one presented here. Given the dominant contribution of strong lines to the total line flux in this source, an accurate determination of their emission is most important in deriving the necessary correction. Complete and unbiased surveys such as the present work require very large amounts of time and can only be done for selected objects and in selected frequency ranges at present. If the finding that strong lines dominate the line flux holds true in other sources besides IRC +10216, then targeted observations to determine the emission from probable strong lines together with simulations for other species should provide a more practical means of determining the effect of line emission on the dust emissivity in a variety of objects. We also point out that estimating a correction for the integrated line flux in a particular measurement requires a knowledge of the actual passband used as well as the ability to predict the line emission from the source. Even the effective wavelength of the measurement may be affected by the presence of line emission at particular frequencies.

4. SUMMARY

We have carried out a complete spectral line survey over the frequency range 330.2–358.0 GHz with the CSO to a sensitivity level of $T_{MB} \lesssim 95$ mK. An improved deconvolution algorithm has been used to obtain the SSB spectrum over this

range. We detect transitions from eight molecules, all previously known in IRC +10216, with two weak lines remaining unidentified. Column densities and excitation temperatures have been determined using the rotation diagram technique by combining the present data set with published observations at lower frequencies. The derived column densities have been used to determine the relative abundances of the observed species. The resulting values are consistent with previous determinations of abundances in IRC +10216. Emission from molecular lines has been shown to be responsible for the majority of the flux observed with broadband detectors at this frequency. However, LTE simulations of molecular line emission suggest that the contribution of integrated line flux is greatest in this region and drops substantially at higher frequencies. For wavelengths longer than $\sim$750 μm, the molecular line emission may contribute $\gtrsim$50% of the total flux in broadband measurements, making it necessary to correct the observed flux values in order to obtain the flux from the dust. The variation of the dust emissivity with frequency appears likely to be somewhat greater than that found with broadband measurements, when these corrections are made. However, the integrated line flux is dominated by relatively few lines in IRC +10216 so that the precise frequency range included in any flux measurement is critical in determining the actual contribution of line emission to the total flux. Narrowband observations in regions chosen for their lack of lines should be used to obtain the most accurate measurements of the true continuum. Alternatively, it is possible to estimate the amount of flux contributed by lines to broadband observations given the frequency response of the detector. In this case, simulated spectra derived from line catalogs as described herein can provide the necessary line emission information.

We wish to thank the CSO staff for their assistance with the observations. We are grateful to Göran Sandell for permission to use his unpublished data and to an anonymous referee for suggesting the identification of the vibrationally excited $H^{13}CN$ line. This work has been supported by NSF grant AST 90-15755 to the California Institute of Technology. G.A.B. would like to acknowledge support from the David and Lucille Packard and Alfred P. Sloan Foundations.

REFERENCES

Avery, L. W. 1987, in IAU Symp. 120, Astrochemistry, ed. M. S. Vardya & S. P. Tarafdar (Dordrecht: Reidel), 357
Avery, L. W., et al. 1992, ApJS, 83, 363
Becklin, E. E., Frogel, J. A., Hyland, A. R., Kristian, J., & Neugebauer, G. 1969, ApJ, 158, L133
Bieging, J. H., & Nguyen-Q-Rieu 1988, ApJ, 329, L107
———. 1989, ApJ, 343, L25
Blake, G. A., Sutton, E. C., Masson, C. R., & Phillips, T. G. 1986, ApJS, 60, 357
Campbell, M. F., et al. 1976, ApJ, 208, 396
Carter, S., Mills, I. M., & Handy, N. C. 1993, J. Chem. Phys., 99, 4379
Cernicharo, J., & Guélin, M. 1987, A&A, 183, L10
Cernicharo, J., Guélin, M., Kahane, C., Bogey, M., Demuynck, C., & Destombes, J. L. 1991, A&A, 246, 213
De Lucia, F. C., & Helminger, P. A. 1977, J. Chem. Phys., 67, 4262
Ellison, B. N., Schaffer, P. L., Schaal, W., Vail, D., & Miller, R. E. 1989, Internat. J. IR MM Waves, 10, 8
Frum, C. I., Engleman, R., Jr., & Bernath, P. F. 1990, J. Chem. Phys., 93, 5457
Glassgold, A. E., Mamon, G. A., Omont, A., & Lucas, R. 1987, A&A, 180, 183
Gottlieb, C. A., Vrtílek, J. M., & Thaddeus, P. 1989, ApJ, 343, L29
Greaves, J. S., & White, G. J. 1991, A&AS, 91, 237
Groesbeck, T. D., Phillips, T. G., & Blake, G. A. 1994, in preparation
Grossman, E. N. 1989, AT atmospheric transmission software, Airhead Software, 2069 Bluff St., Boulder, CO 80304
Guélin, M., Cernicharo, J., Navarro, S., Woodward, D. R., Gottlieb, C. A., & Thaddeus, P. 1987, A&A, 182, L37
Huggins, P. J., Olofsson, H., & Johansson, L. E. B. 1988, ApJ, 332, 1009
Jewell, P. R., Hollis, J. M., Lovas, F. J., & Snyder, L. E. 1989, ApJS, 70, 833
Johansson, L. E. B., et al. 1984, A&A, 130, 227
Kahane, C., Cernicharo, J., Gomez-Gonzalez, J., & Guélin, M. 1992, A&A, 256, 235 (K2)
Kahane, C., Gomez-Gonzalez, J., Cernicharo, J., & Guélin, M. 1988, A&A, 190, 167 (K1)
Kwan, J., & Linke, R. A. 1982, ApJ, 254, 587
Lucas, R. 1992, in IAU Symp. 150, Astrochemistry of Cosmic Phenomena, ed. P. D. Singh (Dordrecht: Reidel), 389
Lucas, R., & Cernicharo, J. 1989, A&A, 218, L20
Lucas, R., & Guilloteau, S. 1992, A&A, 259, L23
McCabe, E. M., Smith, R. C., & Clegg, R. E. S. 1979, Nature, 281, 263
Morris, M. 1975, ApJ, 197, 603
Olofsson, H., Johansson, L. E. B., Hjalmarson, Å., & Nguyen-Q-Rieu. 1982, A&A, 107, 128
Omont, A. 1987, in IAU Symp. 120, Astrochemistry, ed. M. S. Vardya & S. P. Tarafdar (Dordrecht:Reidel), 357
Penzias, A. A., & Burrus, C. A. 1973, ARA&A, 11, 51
Poynter, R. L., & Pickett, H. M. 1985, Appl. Opt., 24, 2235
Sopka, R. J., Hildebrand, R., Jaffe, D. T., Gatley, I., Roellig, T., Werner, M., Jura, M., & Zuckerman, B. 1985, ApJ, 294, 242
Sutton, E. C., Blake, G. A., Masson, C. R., & Phillips, T. G. 1984, ApJ, 283, L41
———. 1985, ApJS, 58, 341
Sutton, E. C., Jaminet, P. A., Danchi, W. C., & Blake, G. A. 1991, ApJS, 77, 255
Thaddeus, P., Cummins, S. E., & Linke, R. A. 1984, ApJ, 283, L45
Truong-Bach, Nguyen-Q-Rieu, Omont, A., Olofsson, H., & Johansson, L. E. B. 1987, A&A, 176, 285
Turner, B. E. 1987a, A&A, 182, L15
———. 1987b, A&A, 183, L23
———. 1989, ApJS, 70, 539
Walker, C. K., Groesbeck, T. D., & Blake, G. A. 1994, in preparation
Walmsley, C. M., Chini, R., Kreysa, E., Steppe, H., Forveille, T., & Omont, A. 1991, A&A, 248, 555
Wang, V. K., & Overend, J. 1973, Spectrochim. Acta, 29A, 687
Williams, P. G., & White, G. J. 1992, A&A, 266, 365 (WW)
Wootten, A., Lichten, S. M., Sahai, R., & Wannier, P. G. 1982, ApJ, 257, 151
Ziurys, L. M., & Turner, B. E. 1986, ApJ, 300, L19